Ultrafast Dynamics in Superexcited States of Phenol

Carolyn P. Schick and Peter M. Weber*

Department of Chemistry, Brown University, Providence, Rhode Island 02912

Received: September 16, 2000; In Final Form: January 23, 2001

We observe three-photon ionization photoelectron spectra of phenol in a molecular beam. After excitation by the first photon to the S_1 electronic state, a second photon lifts the molecule to a set of superexcited molecular states at an energy of 9 eV, which is 0.5 eV above the ionization energy. Photoelectron spectra are obtained by ionizing the molecule with a third photon. The spectra show prominent Rydberg series with $\delta = 0.32$ and $\delta = 0.80$, as well as several other series. Time-delayed photoelectron spectra are obtained from two-color ionization experiments. These spectra are analyzed by eliminating underlying contributions from competing ionization processes, and by referencing all decays to a set of particularly persistent photoelectron peaks. A kinetic picture emerges that invokes an ultrafast conversion of the initially excited, optically bright, superexcited valence state to a set of vibrationally excited Rydberg states, on a femtosecond time scale. Further dynamical processes among the Rydberg states proceed on a picosecond time scale.

Introduction

Superexcited states are electronic states of neutral atoms or molecules with an energy above the first ionization energy.[1−4] Examples are Rydberg states that converge to internally excited states of the ion, as well as valence excited states above the ionization energy. Latter states can arise from the excitation of electrons from orbitals lower than the highest occupied molecular orbital (HOMO), or from a 2-fold electronic excitation. While it is expected that a vast number of superexcited states exist in polyatomic molecules, only Rydberg states have been abundantly observed and thoroughly characterized.[5−8] Highly excited valence states, which are, for example, seen in absorption spectra as Feshbach resonances, are comparatively poorly understood. The presence of many nonradiative decay channels causes their lifetimes to be very short. Decay channels include relaxation to the continuum of isoenergetic ion states (autoionization), relaxation to lower-lying vibronic states of the neutral molecule, and reactive pathways resulting in isomerization or fragmentation of the molecule.

While the short lifetimes of superexcited states make them difficult to probe with available experimental techniques, they may indeed be quite relevant in a number of important processes. For example, superexcited states may be involved in the primary step of radiation chemical events. After an energetic particle strikes a molecule, one often observes a range of reaction products, as is abundantly observed in mass spectrometers using electron beam ionization.[9,10] The mechanisms by which these fragments are generated are often obscure, as they do not conform to the rules of solution-phase chemistry. Apparently, energetic particles prepare the molecule in highly reactive electronic states, which then undergo a diverse set of reactions.[11] An understanding of highly excited molecular states and their relaxation pathways is therefore desirable for the elucidation of reaction mechanisms of ion fragmentation.

Superexcited states of molecules may also play a role in modern spectroscopy experiments such as zero kinetic energy (ZEKE) spectroscopy[12] and mass-analyzed threshold ionization (MATI).[13,14] Those experiments employ electronically excited resonances in multiphoton ionization as agents to probe the spectroscopy and structure of molecules or clusters. Clearly, an understanding of how superexcited molecular states affect multiphoton ionization experiments is important to their interpretation. Finally, there are a growing number of experiments performed using time-resolved ionization in an effort to learn about dynamical processes in excited electronic states of molecules.[15−23] Those experiments can be affected by superexcited states, because they provide ionization pathways that compete with the desired ionization mechanism. As we will show, understanding the competing ionization paths is quite important for the analysis of time-resolved multiphoton ionization mass spectrometry and photoelectron spectroscopy.

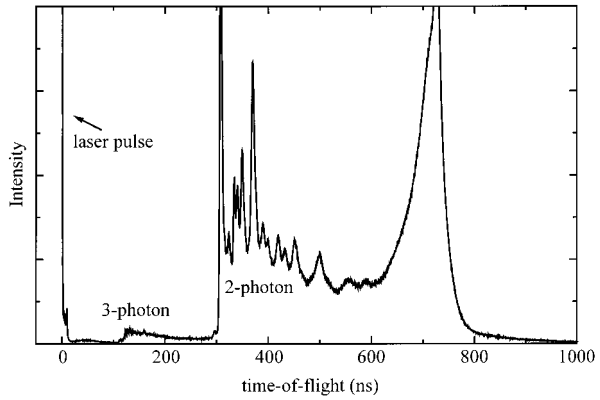

Figure 1. Time-of-flight spectrum of the photoelectrons ejected upon ionization of phenol with 275 nm laser pulses. The peak at time zero is due to scattered laser light. The peak at 700 ns arises from very slow electrons. The electrons in the intermediate regions are due to three-photon and two-photon ionization processes.

In our work, we first noticed evidence for three-photon ionization processes when we observed time-of-flight spectra of electrons that were ejected from phenol upon irradiation with femtosecond laser pulses at 275 nm. Figure 1 shows a time-of-flight spectrum where the 275 nm (4.5 eV) photon is resonant with the origin of the $S_0 \rightarrow S_1$ transition.[24] A second photon of the same energy is sufficient to ionize the molecule, as the ionization energy is at 8.51 eV,[12,25] which is 0.5 eV below the

10.1021/jp003303o CCC: $20.00
Published on Web 03/21/2001

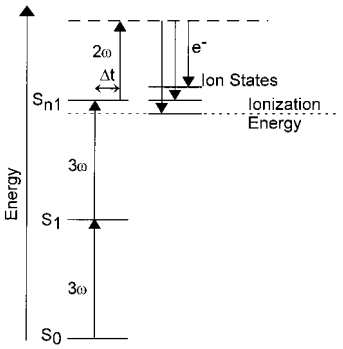

Figure 2. Double-resonance three-photon ionization scheme. The first photon (third harmonic of the laser, 3ω) is resonant with the origin level of the $S_0 \rightarrow S_1$ transition. Two more photons ionize the molecule via a superexcited state near 9 eV. The last step is with either a third- or second-harmonic photon; shown in the figure is a time-delayed second-harmonic (2ω) photon.

combined energy of the two photons. As expected, the electron flight time distribution is dominated by a signal corresponding to the generation of a set of vibrational states of the ion in its ground electronic state. This part of the spectrum, which in our instrument with a 14.54 cm flight distance appears at flight times between 300 and 700 ns, is well understood.[26] The strong, broad peak at 700 ns seen in Figure 1 arises from electrons that are ejected with very small energy. Those electrons are pushed toward the detector by small contact potentials that are present in the ionization region, so that their detection efficiency is very large.[27]

While most of the signal in Figure 1 is well accounted for by established two-photon ionization mechanisms, we observe a most curious set of peaks with flight times that are much shorter than had been previously observed. In Figure 1, this signal is seen between 120 and 200 ns. Upon conversion to an electron energy spectrum, we found that these electrons possess energies up to 5 eV. Clearly, two photons of 4.5 eV each cannot eject electrons with 5 eV of energy from a molecule with an ionization energy of 8.51 eV. Instead, there is evidence that this signal is generated in a double-resonance, three-photon ionization of phenol accessing both the S_1 and a superexcited molecular state. The exploration of this small three-photon signal presents the topic of the present as well as an accompanying paper.[28]

Our experiments are discussed using the three-photon ionization scheme shown in Figure 2. Phenol is excited with two 275 nm (4.5 eV) photons that are generated as the third harmonic (3ω) of the infrared output of a titanium:sapphire laser. A third laser photon ionizes the molecule, and we measure the kinetic energy of the ejected electrons to derive a photoelectron spectrum. The photon used to ionize the molecule is either an additional 3ω photon or, as shown in Figure 2, a second-harmonic (2ω) photon at 413 nm (3.0 eV). Use of the second-harmonic photon allows us to introduce a time delay between preparing and probing the superexcited states, enabling us to observe their time evolution.

In constructing Figure 2, various assumptions are made, which in the present paper we seek to substantiate. Among them are the description of the ionization as a three-photon process rather than a higher order process and the existence of superexcited molecular resonances above the ionization energy. We furthermore seek to understand the nature of the ionization mechanism, the character of the superexcited states involved, and the time scales on which nonradiative processes proceed in superexcited molecules.

After describing the experimental apparatus, we present the results obtained by ionizing phenol in the $3\omega + 3\omega + 3\omega$ and $3\omega + 3\omega + 2\omega$ processes. We also describe related experiments, and show the result of a one-color $2\omega + 2\omega + 2\omega + 2\omega$ ionization as an example. An ionization scheme is discussed that accounts for the observed spectra by invoking an ultrafast relaxation process from an initially prepared, optically bright superexcited state to a set of vibrationally highly excited Rydberg states that are dark in absorption. Finally, while many of the relaxation paths remain beyond the time resolution of our instrument, we observe the kinetics for some components of the decay.

Experimental Details

Our apparatus has been extensively described in previous publications.[15,27,29] Briefly, we use a regeneratively amplified titanium:sapphire laser system (Spectra-Physics) to produce tunable laser pulses between 760 and 840 nm, with durations of 120 fs. The 50 kHz repetition rate of our laser system is favorable because it allows us to use digital detection electronics while enabling efficient harmonic conversion. Typical energies in the infrared are about 8 μJ/pulse. Two nonlinear optical crystals, LBO and BBO, generate harmonics at 413 nm (2ω) and 275 nm (3ω), which we use as probe and pump pulses, respectively. The durations of the 2ω and 3ω pulses were found to be 125 and 180 fs, respectively, as determined by zero-background autocorrelation.

Phenol is seeded at 60 °C in a stream of helium at 1.1 bar. The gas mixture is expanded through a 94 μm nozzle into a three-stage molecular beam apparatus pumped by four turbomolecular pumps. The continuous molecular beam is intersected by the copropagating 3ω and 2ω laser beams, which are each focused to a spot size of about 20 μm. The ionization proceeds in the largely field-free chamber, so that photoelectrons are ejected in all directions, even though there may be some interesting angular distributions associated with the photoemission processes.[30] The arrival times of the photoelectrons with respect to the laser pulses are recorded using digital electronics equivalent to those used in time-resolved single-photon counting. Corrections to the electron flight times, especially important when fast electrons are analyzed, have been described previously.[15] Use of those corrections leads to spectra where the adiabatic ionization energy agrees with literature values to within 30 meV, even when electrons are observed with energies up to 5 eV. The largest remaining sources of error are the channel resolution of the multichannel analyzer (2048 channel depth) and small uncertainties in the arrival time of the laser pulse at the molecular beam. To obtain slightly more accurate photoelectron energies, we adjust the laser pulse arrival times such that the spectra reproduce the literature value for the adiabatic ionization energy of phenol.[12,25]

In the experiments presented here, the polarizations of all laser beams are parallel to the direction of the detector, which, in turn, is perpendicular to the plane spanned by the molecular and laser beams.

Phenol, C_6H_5OH, was purchased from Aldrich and used without further purification. The resonance ionization via an excited electronic state is selective toward the chosen molecule, so that no impurities were expected to contribute to our spectra. Indeed, the mass spectrum observed in our apparatus when ion voltages were turned on showed prominently the phenol parent ion at mass 94. We observed a small amount of fragmentation, with a pattern characteristic of phenol: a very small amount (1.1%) of $C_6H_5O^+$ at mass 93, fragments of $C_5H_6^+$ at mass 66

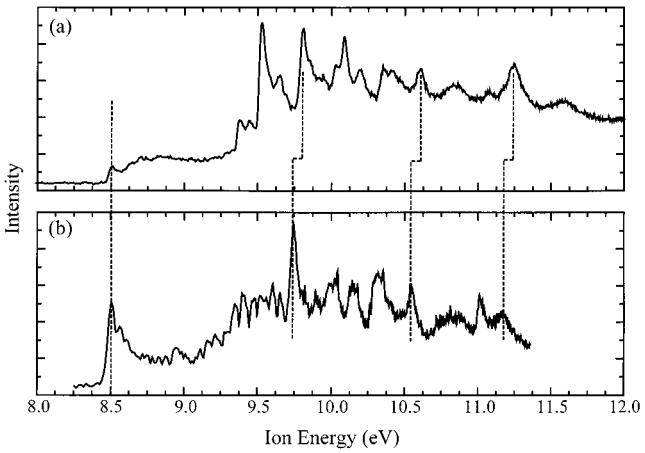

Figure 3. (a) Ionization of phenol with three photons of 4.51 eV each. (b) Ionization of phenol with four photons of 2.99 eV each. Vertical dashed lines illustrate the correspondence between the peaks and highlight a uniform shift of 0.04 eV for the peaks above 9 eV.

(19%) and of $C_5H_5^+$ at mass 65 (1.7%), and some smaller fragments at masses 39, 40, 50, 51, 52, 53, 54, 55, and 56 (4.3% combined). Since our spectrometer was not equipped with a photoelectron−photoion coincidence detection scheme, we could not determine whether the generation of the fragments was related to the three-photon ionization observed in the photoelectron spectra.

Results

Multiphoton Ionization Photoelectron Spectra. To convert a time-of-flight electron spectrum, such as the one shown in Figure 1, to a photoelectron spectrum displaying ion energies, the total absorbed photon energy needs to be known. The observation of electron energies of up to 5 eV implies that phenol absorbs more than two photons, but we have no a priori knowledge whether three or more photons are absorbed. With the assumption of a three-photon ionization process, the time-of-flight spectrum from Figure 1 converts to a photoelectron spectrum as shown in Figure 3a. The spectrum has a sharp onset at 8.51 eV, which coincides with the well-known ionization energy of phenol.[12,25] This suggests that at least the onset of the spectrum in Figure 3a is properly described as an ionization process with three photons of 4.51 eV each. In addition, there is a prominent series of sharp peaks in the energy range from 9.5 to 12 eV. A one-photon photoelectron spectrum, taken with He(I) radiation, shows an unstructured, broad band at 9.40 eV (ionization to $\tilde{A}$ ions), as well a band at 11.59 eV (ionization to $\tilde{B}$ ions).[31,32] The region between those peaks is void of any signal. In contrast, the spectrum in Figure 3a features numerous lines within that range. While this may raise doubts about the assumption of a three-photon ionization mechanism for this section of the spectrum, conclusive evidence in favor of a three-photon ionization is provided by a separate experiment.

When phenol is irradiated with second-harmonic laser pulses at 414 nm, only a very small signal can be observed. The resulting photoelectron spectrum shows that most of that signal is due to a three-photon process, and that the vibrational photoelectron peaks look similar to both a one-photon ionization with a He(I) source and a resonant two-photon ionization with 4.51 eV laser photons. However, a small fraction of the ionization signal arises from much faster electrons, with up to 3.5 eV of energy. This part of the photoelectron spectrum was converted to an energy scale by assuming an ionization process with four photons of 2.99 eV each, resulting in Figure 3b. While the signal is weak, we note that the spectrum in Figure 3b is very similar to the spectrum in Figure 3a. Most of the peaks in the 9.5−11.5 eV range match the ones from Figure 3a, even though, characteristically, all peaks above the ionization onset are shifted by 0.04 eV.

The comparison between parts a and b of Figure 3 supports the postulated $3\omega + 3\omega + 3\omega$ ionization process for Figure 3a and the $2\omega + 2\omega + 2\omega + 2\omega$ ionization scheme for Figure 3b. The similarity of the peak structures indicates that the ionization in each case proceeds out of the same set of molecular states. For the 3ω and 2ω photons to prepare the same set of molecular states, the resonance must be at an energy that is a multiple of both 4.5 and 3 eV. The lowest such energy is at 9 eV. While a higher multiple is mathematically possible, the generation of molecular states at 18 eV or higher seems quite absurd. We therefore invoke the existence of a resonance at an energy of about 9 eV for both spectra shown in Figure 3. The ionization process in Figure 3a uses three photons of 4.51 eV, while the ionization in Figure 3b uses four photons of 2.99 eV. In either case, the ionization uses one more photon than necessary to ionize the molecule.

Note that our argument is that we *observe* the photoelectron spectra from the same set of states. We do not necessarily suggest that the $3\omega + 3\omega$ excitation *prepares* the same initial state as the $2\omega + 2\omega + 2\omega$ excitation. This leaves open the possibility that the optical excitation prepares different states which subsequently decay to the same product states, and that ionization occurs out of the common product states.

It is important to address the possibility that the spectra shown in Figure 3 could result from either an impurity in the sample or a molecular fragmentation. Impurities can be excluded on the basis of the mass spectrum, which shows no signal other than phenol and its characteristic fragments. The signal-to-noise ratio of our mass spectrometer is very high, $>10^5$, so that impurities would be seen easily.[33] Ionization of fragments does not seem a likely participant in the multiphoton processes. First, the lifetime of the S_1 resonance is about 2 ns. Since we use femtosecond laser pulses to ionize the molecule, there is little opportunity for fragmentation from the S_1 state. Moreover, any fragments that might form would not likely have an ionization energy dramatically lower than the 8.51 eV of phenol. To explain the observation of electrons with kinetic energies of 5 eV, one would still have to postulate a three-photon process, this time involving the fragments. With these considerations in mind, it seems unlikely that we observe anything other than multiphoton ionization photoelectron spectra of phenol.

In addition to the spectra displayed in Figure 3, we have observed similar spectra when ionizing via the S_2 electronic resonance. Those spectra use the fourth harmonic (4ω) of the laser at 6.01 eV to prepare the S_2 state, and then ionize with two second-harmonic photons of 3.01 eV each ($4\omega + 2\omega + 2\omega$). The 6.01 eV plus 3.01 eV photons lead again to an excitation at 9.02 eV. We observe photoelectron spectra that are strikingly similar to the ones described in this paper, in further support of the interpretation presented here. Those spectra, as well as their dependence on the delay between the 4ω and 2ω photons, are described in a separate paper.[28]

Multiphoton ionization spectra were also obtained via several vibrational resonances in the S_1 electronic state. As the 3ω wavelength was reduced to match higher vibrational levels in S_1, the sharp peaks from 9.5 to 11.5 eV retained their intensity distribution, but shifted in energy by an amount corresponding to the change in the two-photon excitation energy. The same effect is observed when the spectra of Figure 3 are compared:

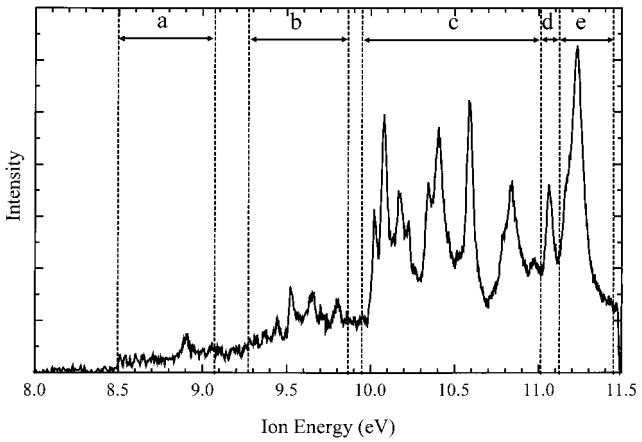

Figure 4. Two-color ionization photoelectron spectrum of phenol near time zero. The vertical dashed lines identify regions a (from 8.50 to 9.07 eV), b (from 9.27 to 9.86 eV), c (from 9.95 to 11.02 eV), d (from 11.02 to 11.13 eV), and e (from 11.13 to 11.46 eV).

while the peak intensities and relative positions of the peaks are quite similar in parts a and b of Figure 3, all peaks in the 9.5−11.5 eV range in Figure 3b are shifted to lower energy by 0.04 eV. As discussed later, this shift arises from the slightly different energies of the photons that prepare the superexcited state.

Time-Resolved Photoelectron Spectra. Ionization using the two-color $3\omega + 3\omega + 2\omega$ scheme allowed us to introduce a delay time between the two-photon excitation with 3ω and the ionization with 2ω. The photoelectron spectrum near time zero is shown in Figure 4. It features the same spectral bands as before, although with a different intensity distribution. The spectral resolution of Figure 4 is better than that of Figure 3a because the ionization produces slower photoelectrons that can be more accurately measured with our time-of-flight instrument.

The two-color scheme enables us to map the time evolution of participating states by delaying the second-harmonic probe pulse with respect to the third-harmonic pulse. Ideally, in the absence of laser power fluctuations, a measurement of time-delayed photoelectron spectra could be made with our apparatus by either observing a photoelectron peak and changing the delay time or setting the delay time to a specific value and measuring the entire spectrum. However, slight laser power fluctuations did exist, and the processes under investigation were extremely nonlinear with respect to the laser power. Thus, while the two choices gave results that were in general agreement, they were of very different quality.

Our initial efforts focused on collecting time-delay scans by gating on a specific photoelectron peak and measuring its time dependence by scanning the 2ω delay time. While these experiments resulted in decay curves of reasonable quality, pursuit of the second method revealed systematic problems that shed some doubt on the utility of the time-delay scans for measuring the kinetics of the superexcited states.

In the second approach we measured photoelectron spectra at various delay times and then analyzed them to obtain the time dependence of individual peaks. Twelve spectra were taken, with time delays up to 6.2 ps. Fluctuations of the laser power caused a loss of an intensity relation between the different spectra. That is, there were 11 scaling factors that related the experimentally measured intensities, and which needed to be determined to extract the time dependence.

To determine the scaling factors, we divided the spectrum shown in Figure 4 into five regions, labeled a−e. Peaks within those regions were found to exhibit an identical time evolution.

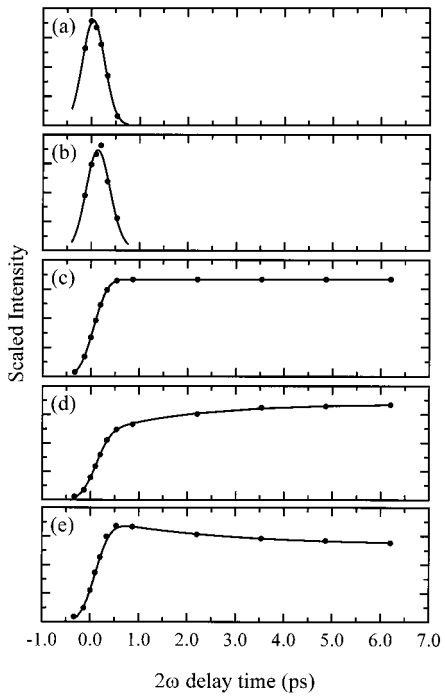

Figure 5. Scaled intensity plots versus time delay for regions a−e as indicated in Figure 4. The experimental data were corrected by the scaling multipliers to remove spurious noise. The solid line shows the fit for each region. Note that region c serves to determine the scaling multipliers, and therefore shows no deviation between the measured data and the fit.

From a further experiment with 2.9 s time delay, we noted that the signal of region c persisted into the nanosecond regime. This implied little change on a picosecond time scale, an observation that was supported by the time-delayed experiments. The persistence of the region c signal provided an internal calibration that enabled us to normalize for intensity fluctuation between spectra: we modeled the rise of the region c signal using a single exponential, and assumed that on the picosecond time scale there was no decay. The deviations between the experimentally measured region c signal and the modeled region c signal then provided scaling factors that enabled us to normalize the intensities of the 12 different spectra. From the normalized spectra, it was then possible to measure the kinetics of all five spectral regions. A detailed description of the analysis procedure is made available as Supporting Information.

In Figure 5, panels a−e show the measured data for the respective regions, after multiplication by the set of 11 multipliers obtained by our procedure. The panels also show the fits to the data. It should be noted that the overall signals for regions a and b were extremely small, and in those curves we found some residual scatter about the theoretical curves. For region d, the fit was nothing short of excellent. The fit of region e was again very good, although there was a small deviation at delay times between 400 and 600 fs. This deviation is not likely due to an error in the fit, or instrumental noise. Much rather, it arises from a shortcoming of the single-exponential forms chosen to describe the kinetics of the different regions, suggesting a more complicated kinetic model. Nonetheless, the deviation was not deemed significant enough to warrant inclusion of further terms in the theoretical expressions for region c or e.

From the fits, we obtained a width of 230 fs for the instrument function. We determined an admixture of 20% of the b region signal to region c, and an admixture of the type c signal to regions d and e of 41% and 59%, respectively. These admixtures

are explained by overlapping spectral signatures of different ionization pathways, as discussed below. Within the available time resolution, we were not able to resolve either the rise or the decay of region a. The rise of region b was also too fast to measure, but for its decay we obtained a value of 9×10^{12} s^{-1}. Given the duration of the instrument function of 230 fs, this value should be considered approximate. The region c signal rises well within the laser pulse; the fit gave a value of 1.4×10^{13} s^{-1}, but that must also be considered too fast to measure accurately. The region d signal rises with a rate of 5.5×10^{11} s^{-1}, and does not decay on the picosecond scale. Finally, region e rises within the instrument function (fit: 1×10^{13} s^{-1}) and decays with a rate of 3.9×10^{11} s^{-1}.

Discussion

The multiphoton ionization photoelectron experiments of phenol show richly structured spectra at energies where no photoelectron peaks have previously been observed. In this section we explore their interpretation and assignments, and the dynamical processes that ensue when phenol is prepared in the superexcited state.

Nature of the States Seen in the Photoelectron Spectra. The part of the spectrum that stretches from 8.5 to 9 eV, labeled region a in Figure 4, is quite straightforward to understand. The resolution of our photoelectron spectrometer for the 5 eV kinetic energy electrons is fairly low, and the signal seen below 9 eV in Figures 3 and 4 is quite small. Nevertheless, we can identify a Franck−Condon envelope that is similar to the one observed when ionizing phenol from either the ground electronic state[32] or the S_1 electronic state.[15,26] The strongest individual peak in that region is at 8.51 eV—the origin energy for phenol ground-state ions. This suggests that the Franck−Condon factor to the vibrationless level in $\tilde{X}$ is large, which is consistent with only a small change in the shape of the potential energy surfaces. This suggests an ionization mechanism where the first 3ω photon excites the $S_0 \rightarrow S_1$ transition, promoting an electron from the HOMO to the LUMO. Two more photons then eject the electron from the LUMO in an above-threshold ionization (ATI) process. ATI processes have been observed on many occasions when molecules are ionized by high-intensity laser pulses.[34−37] The intensity of our laser pulses at the focus is estimated to be 5×10^{11} W/cm^2, which is at the borderline where ATI sets in. In above-threshold ionization, one typically observes a series of photoelectron peaks, with energy spacings equaling the energy of the ionizing photon. The ionization is sudden, and Franck−Condon factors govern the vibrational intensity distributions. The Franck−Condon envelopes seen in Figures 3 and 4 are consistent with an interpretation of the region a signal as due to an ATI process. The time-resolved experiments were not able to detect either a rise or a decay of the region a signal, which is again consistent with the ATI mechanism. We are thus confident that the very small signal observed below 9 eV is properly understood as above-threshold ionization.

The peaks that dominate the spectrum, above 9 eV, cannot arise from ATI for three reasons: (1) there are no matching ion states known in that region, (2) the peaks do not appear to be shifted by multiples of the ionizing photon energy, and (3) the peaks exhibit a time dependence on a femtosecond to nanosecond scale. For these peaks a more elaborate model needs to be constructed.

Our interpretation of the spectral regions b−e is guided by the following observations. Most of the signal in these regions consists of sharp peaks. There are no obvious constant spacings between peaks as one would expect for vibrational progressions. The photoelectron peaks shift with the energy of the laser photons, suggesting that nonradiative processes are involved. And the peaks in region c persist on a nanosecond time scale.

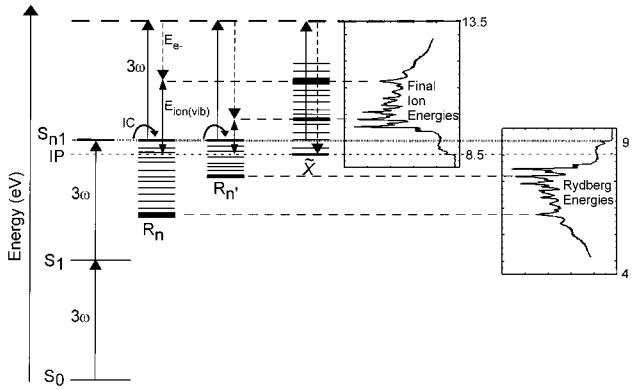

Figure 6. Schematic diagram showing three-photon ionization of phenol at 275 nm. This energy diagram corresponds to the process occurring in Figure 3a. R_n and $R_{n'}$ represent just two of the many Rydberg states accessed by electronic relaxation from the superexcited state, S_{n1}. The resulting photoelectron spectra can be analyzed to show the final ion energies, left spectrum, or the energies of the Rydberg states, right spectrum.

To explain the three-photon ionization photoelectron spectra, we propose a model that invokes a resonant two-photon excitation to a primary superexcited state at 9 eV, followed by a subsequent relaxation to isoenergetic vibronic levels of the neutral molecule. The ionization proceeds from the states that are populated during the electronic relaxation process. This scheme is illustrated in Figure 6.

The first two steps of the three-photon ionization scheme prepare a primary superexcited state, S_{n1}, in a resonance excitation via the S_1 electronic state. The nature of this primary superexcited state is discussed below. It is postulated to carry the oscillator strength from the S_1 electronic level, and to have a short lifetime. Many decay channels are open to this superexcited state. The channel that leads to the observed spectra is a relaxation to a set of isoenergetic molecular Rydberg states. Figure 6 illustrates only Rydberg states that converge to the ground electronic state of the ion, but in general, Rydberg states converging to excited phenol ions could play a role as well. The third photon ionizes the molecule from those Rydberg states.

As is usual in electronic relaxation processes, the difference in the electronic energies of the primary superexcited state and the Rydberg states is converted to vibrational excitation. This vibrational energy remains with the molecule in the ionization step. The phenol ions are therefore generated with a large amount of vibrational energy, depending on the particular Rydberg state involved.

Electronic relaxation processes have frequently been witnessed in multiphoton ionization photoelectron spectroscopy.[15,16,18,19,21−23,38] If the relaxation is very fast, only the product states are observed,[39,40] but if relaxation is slower than the instrument function, then the flow of energy as a function of time can be resolved. In most experiments, ionization out of the relaxed electronic states leads to broad bands in the photoelectron spectra. This is due to differences in the shapes of the potential energy surfaces between the neutral molecule and the ion. Those differences give rise to a dispersion of the transition energies when vibrational quantum numbers are conserved, and permit transitions that do not conserve vibrational quantum numbers. Because electronic relaxation is usually a

nonradiative process in the statistical limit,[41] a very large number of transitions are observed, each with a slightly different energy.

Our model suggests that the nonradiative decay of the primary, optically bright superexcited state leads to a set of isoenergetic, vibrationally excited Rydberg states. The potential energy surfaces of Rydberg states closely approximate the surfaces of the ion states to which they converge. As a result, ionization from a vibrationally excited Rydberg level conserves the vibrational quantum numbers, and the transition energy does not depend on the nature of the particular vibration that is excited.[42] Thus, even though the nonradiative decay of the primary superexcited state to a particular Rydberg state populates many isoenergetic vibrational states, the photoionization does not alter the vibrational energy content, and the ions are generated in isoenergetic vibrational states. Consequently, the photoelectron spectrum features sharp peaks, each representing one Rydberg level.

The model for the three-photon ionization allows us to derive the electronic energies of the Rydberg levels relative to their respective ion energies. The combined energy of the three photons must equal the total energy of the ion (electronic and vibrational) plus the energy of the ejected electrons. For ionization in the $3\omega + 3\omega + 3\omega$ scheme we have

$$3\hbar\omega_3 = E_{\text{ion(elec)}} + E_{\text{ion(vib)}} + E_{e^-} \qquad (1)$$

Here, $\hbar\omega_3$ is the energy of the third-harmonic photon. Independent of the nature of the primary superexcited state, after the relaxation the electronic energy of the Rydberg state, $E_{R_n(\text{elec})}$, plus its vibrational energy, $E_{R_n(\text{vib})}$, must equal the two-photon excitation energy:

$$2\hbar\omega_3 = E_{R_n(\text{elec})} + E_{R_n(\text{vib})} \qquad (2)$$

Combining eqs 1 and 2, and setting the vibrational energy of the Rydberg state equal to that of the ion state, we obtain

$$E_{\text{ion(elec)}} - E_{R_n(\text{elec})} = \hbar\omega_3 - E_{e^-} = R/(n-\delta)^2 \qquad (3)$$

Here, we have inserted the expression for the energies of the Rydberg levels as a function of their principal quantum number, n, and the quantum defect, δ.[5−8] The quantum defect is a constant that depends on the symmetry of the Rydberg orbital. R is the Rydberg constant, 13.606 eV. While the photoelectron spectra do not provide the final electronic energy of the ion, $E_{\text{ion(elec)}}$, we measure directly the photon energy, $\hbar\omega_3$, and the kinetic energy of the photoelectrons, E_{e^-}. We are thus able to calculate experimental values of $\hbar\omega_3 - E_{e^-}$, which, according to the model, should fit the Rydberg formula with integers n and constant values of δ. Table 1 presents a list of the photoelectron peak energies ($3\hbar\omega_3 - E_{e^-}$) and the ionization energies of the Rydberg levels ($\hbar\omega_3 - E_{e^-}$) measured in the one-color photoionization of the $3\omega + 3\omega + 3\omega$ process, with a two-photon energy of $2\hbar\omega_3 = 9.02$ eV. Included in the table are the values of $n - \delta$.

There are at least two series with constant δ. Combining the data from the $3\omega + 3\omega + 3\omega$, $3\omega + 3\omega + 2\omega$, $2\omega + 2\omega + 2\omega + 2\omega$, and $4\omega + 2\omega + 2\omega$ spectra, we find average δ values of series I to be 0.80 and δ values of series II to be 0.32, both with a standard deviation of 0.01. (The errors in our measurements are large for high n values due to the nonlinear relation between the photoelectron energy and δ and for small n values because most of those peaks are broad. The quoted quantum defect values were calculated for the middle range, with principal quantum numbers of 4−6). There also appear to be several quantum defect values that have no match in either of those Rydberg series. The missing members of these series with higher n values may be obstructed by the intense peaks of the other series.

TABLE 1: Analysis of the Peaks in the $3\omega + 3\omega + 3\omega$ Photoelectron Spectrum[a]

$3\hbar\omega_3 - E_{e^-}$	$\hbar\omega_3 - E_{e^-}$	$n\text{-}\delta = (R/(\hbar\omega_3 - E_{e^-}))^{1/2}$	assignment
9.38	0.36	6.12	series I; $n = 7$, $\delta \approx 0.78$
9.44	0.42	5.67	series II; $n = 6$, $\delta = 0.33$
9.53	0.51	5.17	series I; $n = 6$, $\delta = 0.83$
9.65	0.63	4.66	series II; $n = 5$, $\delta = 0.34$
9.81	0.79	4.15	series I; $n = 5$, $\delta = 0.85$
9.94	0.92	3.84	
10.03	1.01	3.67	series II; $n = 4$, $\delta = 0.33$
10.08	1.06	3.58	
10.20	1.18	3.40	
10.36	1.34	3.19	series I; $n = 4$, $\delta = 0.81$
10.42	1.40	3.12	
10.60	1.58	2.94	
10.85	1.83	2.73	
11.07	2.05	2.58	
11.24	2.22	2.48	
11.58	2.56	2.30	
11.98	2.96	∼2.14	

[a] Listed are the final ion energies ($3\hbar\omega_3 - E_{e^-}$), referenced to the ground state of the molecule, and the observed values of $\hbar\omega_3 - E_{e^-}$, both in electron volts. The values for $n - \delta$, obtained by solving eq 3, with the measured electron energy, E_{e^-}, and $\hbar\omega_3 = 4.51$ eV are shown, as well as assignments to Rydberg series.

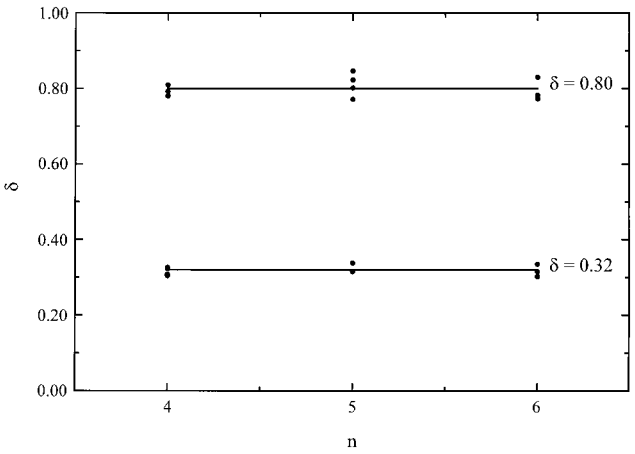

Figure 7. Data points for n and δ, for n from 4 to 6 and δ values of 0.80 and 0.32. Included are data from the spectra obtained in the $3\omega + 3\omega + 3\omega$, $3\omega + 3\omega + 2\omega$, $2\omega + 2\omega + 2\omega + 2\omega$, and $4\omega + 2\omega + 2\omega$ photoionization schemes.

For very low quantum numbers, the Rydberg formula is not expected to be rigorously valid. As a result, we do not expect the quantum defects for small n to fit neatly into Rydberg series.[49] For the peaks with identified quantum defects, we illustrate in Figure 7 the excellent agreement of the calculated values with the spectra. While we cannot identify and assign all the peaks to Rydberg series, we suggest that the good fit of many observed peaks to Rydberg series is evidence in support of our model for the three-photon ionization via superexcited molecular resonances.

Figure 8 illustrates the assignment of the observed photoelectron peaks to Rydberg series with constant δ. The two prominent series have members with $n = 4$ to $n = 6$, with quantum defects of 0.80 and 0.32, respectively. For molecules composed of second-row atoms, typical δ values are 0.9−1.2 for s orbitals, while the δ values of p orbitals are about 0.3−

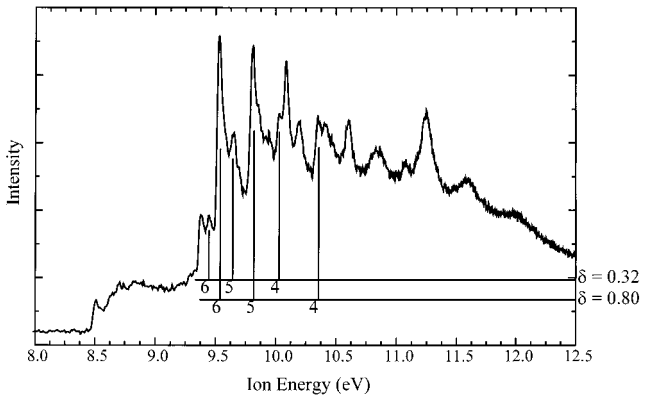

Figure 8. Assignment of Rydberg series with selected n and δ values for the three-photon ionization in the $3\omega + 3\omega + 3\omega$ scheme.

0.5.[43] Apparently, series I corresponds to *n*s states, while series II arises from *n*p Rydberg states. In a similar way, the peaks observed in the other spectra, Figures 3b and 4, can be assigned to Rydberg series. As illustrated in Figure 7, quantum defects derived from the other spectra are, within the errors of our spectral resolution, identical to those reported in Table 1.

The peaks with small principal quantum numbers, seen at high energy in Figures 3, 4, and 8, feature a significant broadening, suggesting a dispersion of vibrational energies upon ionization. This is consistent with their assignment as low quantum number members of the Rydberg series, as one might expect there to be a slight bonding or antibonding character of the Rydberg electrons. The one exception is the peak at 11.07 eV (region d), which also stands out by its slow rise time. As we show in a companion paper,[28] this peak distinguishes itself by its polarization properties as well.

Having assigned the peaks between 9.5 and 11.5 eV to Rydberg series, we next discuss to which electronic state of the ion the series might converge. It is likely that the ground electronic state of the ion, the $\tilde{X}$ state, is associated with at least some of the observed Rydberg series. The $\tilde{A}$ state of the ion has an energy of 9.4 eV, and some of its Rydberg states are therefore within reach of the nonradiative decay. However, the lack of vibrational resolution in either the He(I) photoelectron spectra[31,32] or the two-photon ionization photoelectron spectra[15] indicates that the $\tilde{A}$ state has a very short lifetime. If that is the case, then the Rydberg states converging to $\tilde{A}$ presumably would be short lived as well. Therefore, states converging to $\tilde{A}$ are unlikely, because our spectra feature narrow lines.

He(I) spectra show the $\tilde{B}$ electronic state of phenol ions at 11.59 eV,[32] with the origin of this state being reported at 11.12 eV.[13] Most of the photoelectron peaks that we observe are below this energy, and therefore cannot be ascribed to Rydberg series converging to $\tilde{B}$ ions. The peaks above 11.12 eV, namely, the ones at 11.24, 11.58, and 11.98 eV, can only be assigned to $\tilde{B}$ ions if one accepts that the vibrational energy they receive in the electronic relaxation process is quite small. Thus, while those few peaks could technically be associated with the $\tilde{B}$ state ions, the vast majority of the remaining peaks certainly cannot be ascribed to $\tilde{B}$ state ions.

Last, given the amount of energy available to the molecule upon two-photon excitation, it is conceivable that nonradiative processes generate isomers of the phenol ion.[44−46] While this indeed is a possibility, any such isomerization would have to proceed on a subpicosecond time scale, since only the peak at 11.07 eV (region d) has a rise time exceeding 1 ps. It thus appears that isomerization is not involved in the spectra that we observe. We conclude that most likely the majority of the peaks observed in the range of 9.5−11 eV arise from Rydberg states that are associated with the ground state of the phenol ion.

Returning now to Figure 6, we see that the kinetic energy spectrum of the photoelectrons can be interpreted in two distinct ways. On one hand, if only electronic ground-state ions are involved, the peaks show ions that are generated with very specific vibrational energies (left spectrum). This spectrum shows the vibrational energy of ions that are generated in the three-photon ionization with intermediate electronic relaxation to Rydberg states. It does not reflect specific ion vibrations, but rather the amount of vibrational energy that is transferred to Rydberg levels in the electronic relaxation process. On the other hand, the observed kinetic energy distribution of the photoelectrons can also be interpreted as a spectrum of Rydberg levels. Using eq 3 and taking the electronic energy of the ions, $E_{\mathrm{ion(elec)}}$, equal to the ionization energy (IP) of the molecule (8.51 eV), we obtain the energies of the Rydberg levels as $\mathrm{IP} - \hbar\omega_2 + E_{e^-}$, where $\hbar\omega_2$ represents the second-harmonic photon that causes ionization. This spectrum, which is a mirror image of the photoelectron spectrum, is shown to the right in Figure 6. From this interpretation we see that the Rydberg levels span an energy range from 5.5 to 8.0 eV.

The last point of this discussion refers to the 0.04 eV shift observed in the spectra between parts a and b of Figure 3. We understand this shift to be a result of the different two-photon excitation energies. The primary superexcited state is generated with an energy of 9.02 eV in Figure 3a and 8.98 eV in Figure 3b. Upon internal conversion, the molecules in the latter spectrum have 0.04 eV less vibrational energy. Since this vibrational energy remains with the molecule, the latter spectrum must be shifted by that precise amount of energy. Thus, our ionization model quite naturally explains the shifts in the photoelectron peaks.

As a final note, we point out that we do not suggest that the three-photon ionization pathway with relaxation to Rydberg states is the exclusive, or dominant, path. There are, of course, two-photon ionization mechanisms, and other relaxation processes such as autoionization and isomerization. These other relaxation pathways quite possibly exist concurrent to the described relaxation to Rydberg states. However, they are not apparent in the three-photon ionization photoelectron spectra.

Primary Superexcited State. Our model rationalizes the photoelectron spectra as arising from the ionization of high-lying, vibrationally excited Rydberg levels. We now examine how those Rydberg levels are populated within the femtosecond time scale of the multiphoton ionization process.

In our experiments, the first photon lifts the molecule from the ground electronic state to the S_1 state, from where it absorbs a second photon. It is unlikely that the absorption from S_1 leads directly to the vibrationally excited Rydberg levels, as the amount of vibrational excitation in those levels is, for some states, very large. For example, a peak observed at 11 eV has a vibrational energy content of 2.5 eV. The ionization from S_1 to the $\tilde{X}$ ions features a strong preference for $\Delta v = 0$ transitions,[15,26] and a similar propensity should be expected for a transition from S_1 to $\tilde{X}$ Rydberg states. Thus, a mechanism other than direct excitation is required.

Our model proposes the existence of a primary, optically bright, superexcited state at 9 eV. This state is quite likely a highly excited valence state. In this scheme, the first step of excitation, $S_0 \rightarrow S_1$, lifts an electron from the HOMO, orbital 18, to the LUMO, orbital 19. It is then possible that a second photon (of the same energy) promotes the remaining electron

from orbital 18 to orbital 19. The resulting state is then described by an electron configuration of $...(16)^2(17)^2(18)^0(19)^2$. Clearly, such a doubly excited valence state has a very short lifetime. Among the many relaxation pathways open to this state are autoionization, where one electron is ejected while the other falls back to orbital 18, and a decay to isoenergetic Rydberg states, where one electron is promoted to a Rydberg orbital while the other falls back to orbital 18. Electrons produced by autoionization would not show up in the three-photon ionization signal. The molecules that decay to a Rydberg orbital can, however, be ionized by a third photon, giving rise to the signal we observe.

As independent support for our model, it would be nice to have absorption spectra of phenol in the S_1 state. Such spectra are unfortunately not available. However, absorption spectra of the phenol ion by Kesper et al.[32] show a strong absorption at 4.5 eV, which they assign to the transition from orbital 18 to orbital 19. Thus, the $18 \rightarrow 19$ transition is at 4.5 eV in both the neutral molecule and the cation, suggesting that the excitation from S_1 to the doubly excited valence state is quite likely also at 4.5 eV. The $S_0 \rightarrow S_1$ transition has a fairly large absorption cross section.[47,48] Inspection of the absorption spectrum of the phenol ion[32] shows that the HOMO−LUMO transition of the ion is also very strong. By extension, it is quite plausible to assume that the excitation from $S_1 \rightarrow S_{n1}$ has a large oscillator strength as well. This may explain why the excitation to the superexcited valence state can effectively compete with the ionization of the molecule out of S_1.

The second step in the electronic excitation of phenol is suggested to be induced by the optically bright character of the S_{n1} state with a configuration of $...(16)^2(17)^2(18)^0(19)^2$. This should not imply, however, that the superexcited valence state is configurationally pure. Indeed, in a separate paper,[28] we describe three-photon ionization experiments via the S_2 electronic state. Those spectra show evidence for a superexcited state at 9 eV as well, and it seems very likely that those experiments involve the same superexcited state as observed here. As laid out in that paper, the orbital character that lends oscillator strength to the $S_2 \rightarrow S_{n1}$ transition is likely a configuration of $...(16)^1(17)^2(18)^2(19)^0(20)^1$. We note that this configuration is a singly excited state that should be accessible from the ground state of the molecule. Indeed, a vacuum ultraviolet absorption spectrum of phenol shows a small peak at 9.0 eV, just where we find evidence for superexcited valence states.[49]

In summary, it is quite likely that the primary superexcited state at 9 eV is a valence state that includes the configurations $...(16)^2(17)^2(18)^0(19)^2$ and $...(16)^1(17)^2(18)^2(19)^0(20)^1$. The doubly excited configuration is the one that provides the oscillator strength for absorption from S_1, while the singly excited configuration is accessed from the S_0 and S_2 levels.

Ultrafast Kinetics of Superexcited Phenol. In the preceding sections we have laid out a model that convincingly explains the three-photon ionization spectra. The focus of the discussion was on the $3\omega + 3\omega + 3\omega$ spectrum, even though the similarity with the spectra obtained in the $2\omega + 2\omega + 2\omega + 2\omega$ and $3\omega + 3\omega + 2\omega$ schemes suggests similar ionization mechanisms. Nevertheless, it is rewarding to examine alternative ionization mechanisms that may take place. This is particularly important for the $3\omega + 3\omega + 2\omega$ process, since we use that ionization scheme to investigate the time evolution of the superexcited levels.

The specific question we pose is whether phenol could be ionized in a three-photon mechanism with one 3ω photon and two 2ω photons ($3\omega + 2\omega + 2\omega$). In this scheme, the first photon prepares the molecule in S_1, and the two subsequent second-harmonic photons ionize it. We note that, with our 50 kHz laser system, off-resonance processes (such as the one discussed in the $2\omega + 2\omega + 2\omega + 2\omega$ ionization process) are extremely weak, so that any $3\omega + 2\omega + 2\omega$ ionization would require a resonance at the $3\omega + 2\omega$ energy, or about 7.5 eV. Indeed, the absorption spectrum of the phenol ion by Kesper et al.[32] shows a prominent absorption band at 3 eV. This absorption is at the same energy as the gap between $\tilde{X}$ and $\tilde{B}$ ions, leading Kesper et al. to suggest a transition from orbital 16 to orbital 18. Because the orbital energy structure of S_1 is quite similar to that of the $\tilde{X}$ ions, as argued above, it is reasonable to suggest that the energy gap between orbitals 16 and 18 in the S_1 state is about 3 eV as well. This opens the possibility that, after initial excitation of the S_1 state by the 3ω photon, a highly excited valence state with the configuration $...(16)^1(17)^2(18)^2(19)^1$, which we call S_{n2}, could be prepared by a 2ω photon. The energy of this state must be at 7.5 eV, which is about 1 eV below the ionization energy. The question is thus whether the two-color spectra show any evidence that a valence excitation at 7.5 eV participates in the doubly resonant ionization process.

A comparison of Figure 4 with Figure 3 reveals no additional peaks in the two-color spectrum. However, while the peak positions agree very well, there is a striking difference in the intensity distribution of the photoelectron peaks. The two-color photoelectron spectrum features a sudden intensity increase for peaks above 10 eV, while the one-color spectra show no corresponding intensity jump. This sudden jump between the regions labeled b and c in Figure 4 may, in fact, be the signature of the proposed $3\omega + 2\omega + 2\omega$ ionization pathway.

The highly excited valence state at a $3\omega + 2\omega$ energy of 7.5 eV has presumably a very short lifetime. On the basis of our earlier discussion, one possible decay mechanism includes electronic relaxation to the Rydberg levels of the molecule. Those Rydberg levels are, of course, the same Rydberg states that are accessed via the 9 eV resonance, with the notable exception that only states with an electronic energy below 7.5 eV can be accessed. Using eq 3, with $E_{\mathrm{ion(elec)}} = 8.5$ eV, $E_{\mathrm{R_n(elec)}} < 7.5$ eV, and $\hbar\omega_2 = 3$ eV, we expect electrons to be ejected with energies $E_{e^-} < 2$ eV. In the photoelectron spectrum analyzed assuming a total photon energy of $3\omega + 3\omega + 2\omega = 12$ eV, those electrons give rise to peaks with ion energies larger than 10 eV. It is precisely at 10 eV where we observe the sudden increase in peak intensities. Thus, at least part of the region c signal can be accounted for by an ionization mechanism using the $3\omega + 2\omega + 2\omega$ scheme. We note that even though it may be surprising that we see the same peak positions in the $3\omega + 2\omega + 2\omega$ ionization scheme as in the $3\omega + 3\omega + 2\omega$ scheme, it follows quite naturally from the postulated ionization mechanism. Specifically, in our interpretation of the photoelectron spectrum as a spectrum of Rydberg levels (right spectrum within Figure 6), the path in which those levels are created, as well as their vibrational energy content, has no effect. We understand this as further evidence for the validity of our model.

The interpretation of the region c signal as arising from an ionization in the $3\omega + 2\omega + 2\omega$ scheme is supported by the absence of any time dependence on a picosecond time scale. The delay between the 3ω and 2ω pulses probes the decay of the S_1 state, and not the decay of a higher excited electronic state. The S_1 state has a decay time of 2 ± 1 ns.[50] This is consistent with our observations, which show that the region c signal survives even in the nanosecond regime, and, in hindsight, justifies our data analysis procedure that ignores any decay of

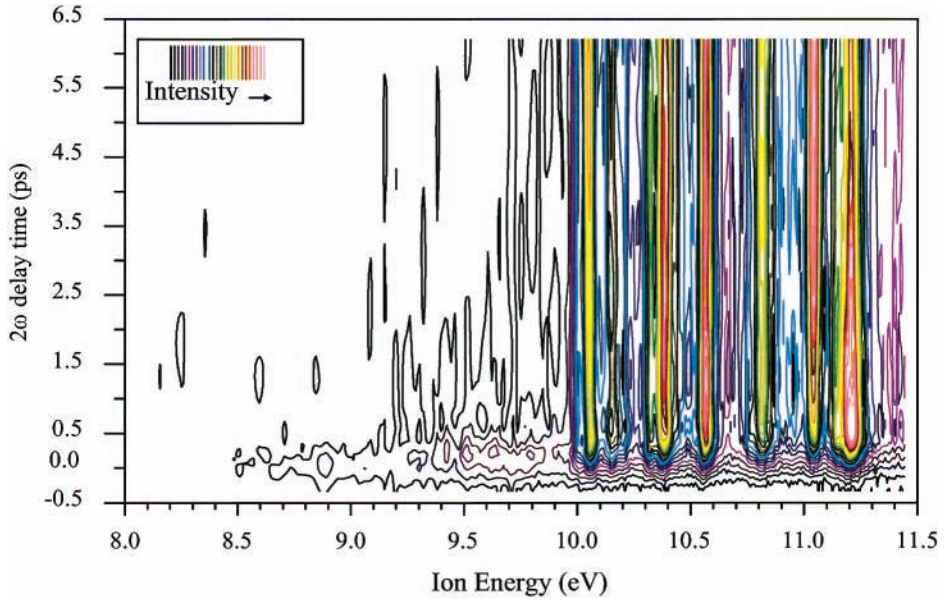

Figure 9. Contour plot of the time-delayed $3\omega + 3\omega + 2\omega$ signal. The axes represent the observed ion energy and delay time, and the intensity of the signal is given by the contours. The scaling multipliers from the data analysis were used to mitigate instrumental noise.

the region c signal on a picosecond time scale. Conversely, the observation of dynamical processes on femtosecond and picosecond time scales implies that the signals in regions a, b, d, and e must arise from ionization in the $3\omega + 3\omega + 2\omega$ scheme. Those signals therefore truly probe the dynamics of superexcited molecular levels on a picosecond and femtosecond time scale.

The analysis described in the Supporting Information allows us to eliminate most of the experimental noise from the measurements, providing multipliers that correct for intensity fluctuations inherent in individual spectra. Using these multipliers, we are able to assemble a composite contour map showing the time dependence of the photoelectron spectrum, shown in Figure 9. The axes represent the photoelectron peak energy and the delay time between the third- and second-harmonic laser pulses. Cross-sectional cuts of the composite map along the energy axis for the different regions, a−e, result in the kinetics curves that are shown in the panels of Figure 5. The contour map emphasizes the dramatic range of time scales encountered in the three-photon ionization of phenol via highly excited valence states and Rydberg states. It furthermore justifies the separation of the spectrum into only five regions, each with a distinct time evolution. As seen in the contour plot, there is little discernible variation in the time evolution of the individual peaks within the regions.

The photoelectron peaks of region b, from 9 to 10 eV, have a lifetime shorter than our instrument can reasonably measure. Evidently, the Rydberg states within this region are generated and decay within our instrument function, or within about 230 fs. The Rydberg peaks of region b arise from levels with principal quantum numbers of 5 and 6. If the $\tilde{X}$ ion is the state to which they converge, then the electronic energies of the Rydberg levels range from 7.5 to 8 eV. Thus, these states require only 0.5−1 eV to autoionize, and their short lifetime may be due to their proximity to the ionization energy. An alternative, or parallel, decay path is the relaxation to lower electronic states.

The photoelectrons observed in region c (10.0−11.0 eV) arise most likely from the $3\omega + 2\omega + 2\omega$ ionization mechanism. Delaying the 2ω from the 3ω pulse therefore does not probe the dynamics of the superexcited molecules. However, we do have information about the kinetics of the peaks in regions d and e. Neither of those peaks is prominent in the spectrum taken at very long delay times. Thus, they decay certainly within nanoseconds. From the fits to our time-resolved photoelectron spectra we derive the decay rate of peak e to be 3.9×10^{11} s^{-1}. A decay of a low-lying Rydberg state on a picosecond time scale can plausibly be explained by an electronic relaxation into a nearby set of lower electronic states. Thus, while autoionization provides a separate decay channel, it appears more likely that further nonradiative electronic relaxation causes the decay of the region e peaks.

Peak d shows only a rise within the picosecond range that is plotted in Figure 9. Our fit gave a rate of 5.5×10^{11} s^{-1}. While this is similar to the decay rate of peak e, given the assumptions of single-exponential rises and decays of the photoelectron peaks, the rise time of peak d is distinct from the decay rate of peak e. It is not clear why only peak d shows a slow rise time. One might speculate that there are sequential nonradiative processes that carry the molecule through the set of Rydberg states. Alternative schemes may involve isomerization or fragmentation of the molecule, in which case the region d peak might correspond to the isomer or fragment. Unfortunately, at the present time there is no independent experimental evidence supporting such scenarios.

Conclusions

We have found evidence for superexcited states of phenol at an energy of 9 eV above the ground state of the molecule. The states are prepared by a resonant two-photon excitation via the vibrationless level of the S_1 electronic state and observed in the photoelectron spectrum upon ionization with a third photon. Using a two-color scheme, we were able to map the time evolution of some of the superexcited states on a femtosecond and picosecond time scale.

The three-photon ionization photoelectron spectra do not show previously unknown electronic or vibrational states of the phenol ion. Instead, they reveal ultrafast relaxation processes within isoenergetic superexcited states of the molecule. A model is proposed in which absorption of a photon from the S_1 state is induced by an optically bright valence state that carries the oscillator strength on account of a partial doubly excited character. This initially prepared superexcited valence state is

very short lived. It decays into a set of vibrationally excited Rydberg states, ionization of which leads to the observed spectra. We used an elaborate data analysis procedure to eliminate noise from the experimental spectra and extract the time scales of the kinetics processes, to the extent that they were within the range of our instrument. Finally, we were able to assign many of the observed states to Rydberg series and found quantum defects that are consistent with those observed in other molecules.

Our work has shed a glimpse of light on the interplay of highly excited molecular states with femtosecond resonance-enhanced multiphoton ionization. Highly excited states are difficult to describe theoretically, and challenging to observe experimentally. Nonetheless, they may be very important to our understanding of primary processes in radiation chemistry, and they may play an important role in the residual fragmentation that is observed in the multiphoton ionization mass spectra with femtosecond laser pulses. Finally, these states complicate the analysis of new and elegant techniques to probe the spectroscopy and dynamics of molecules in transient states using photoelectron spectroscopy. This last point is treated in a separate paper.[28]

Acknowledgment. This research was supported, in part, by funding from the Army Research Office (Grants DAAH04-96-1-0188 and DAAD19-00-1-0141). C.P.S. acknowledges support through a Rhode Island NASA Space Grant Fellowship (Grant NGT5-90014).

Supporting Information Available: A description of the data analysis procedure, including two figures. This material is available free of charge via the Internet at http://pubs.acs.org.

References and Notes

(1) Eland, J. H. D. *Photoelectron Spectroscopy*; Butterworth: London, 1984.
(2) Berkowitz, J. *Photoabsorption, Photoionization, and Photoelectron Spectroscopy*; Academic Press: New York, 1979.
(3) Platzman, R. L. *Radiat. Res.* **1962**, *17*, 419.
(4) Platzman, R. L. *Vortex* **1962**, *23*, 372.
(5) Gallagher, T. F. *Rydberg Atoms*; Cambridge University Press: New York, 1994.
(6) Robin, M. B. *Higher Excited States of Polyatomic Molecules*; Academic Press: New York, 1974.
(7) Robin, M. B. *Higher Excited States of Polyatomic Molecules*; Academic Press: New York, 1975.
(8) Freund, R. S. In *Rydberg States of Atoms and Molecules*; Stebbings, R. F., Dunning, F. B., Eds.; Cambridge University Press: New York, 1983; pp 355−390.
(9) Duckworth, H. E.; Barber, R. C.; Venkatasubramanian, V. S. *Mass Spectroscopy*, 2nd ed.; Cambridge University Press: New York, 1986.
(10) Märk, T. D. In *Electron−Molecule Interactions and their Applications*; Christophorou, L. G., Ed.; Academic Press: New York, 1984; Vol. 1, pp 251−334.
(11) Zipf, E. C. In *Electron−Molecule Interactions and their Applications*; Christophorou, L. G., Ed.; Academic Press: New York, 1984; Vol. 1, pp 335−401.
(12) Müller-Dethlefs, K.; Schlag, E. W. *Annu. Rev. Phys. Chem.* **1991**, *42*, 109.
(13) LeClaire, J. E.; Anand, R.; Johnson, P. M. *J. Chem. Phys.* **1997**, *106*, 6785.
(14) Taylor, D. P.; Johnson, P. M. *J. Chem. Phys.* **1993**, *98*, 1810.
(15) Schick, C. P.; Carpenter, S. D.; Weber, P. M. *J. Phys. Chem. A* **1999**, *103*, 10470.
(16) Sekreta, E.; Reilly, J. P. *Chem. Phys. Lett.* **1998**, *149*, 482.
(17) Hillenbrand, S.; Zhu, L.; Johnson, P. *J. Chem. Phys.* **1990**, *92*, 870.
(18) Smith, J. M.; Zhang, X.; Knee, J. L. *J. Phys. Chem.* **1995**, *99*, 1768.
(19) Cyr, D. R.; Hayden, C. C. *J. Chem. Phys.* **1996**, *104*, 771.
(20) Davies, J. A.; LeClaire, J. E.; Continetti, R. E.; Hayden, C. C. *J. Chem. Phys.* **1999**, *111*, 1.
(21) Radloff, W.; Stert, V.; Freudenberg, T.; Hertel, I. V.; Jouvet, C.; Denonder-Lardeux, C.; Solgadi, D. *Chem. Phys. Lett.* **1997**, *281*, 20.
(22) Fischer, I.; Villeneuve, D. M.; Vrakking, M. J. J.; Stolow, A. *J. Chem. Phys.* **1995**, *102*, 5566.
(23) Blanchet, V.; Zgierski, M. Z.; Seideman, T.; Stolow, A. *Nature* **1999**, *401*, 52.
(24) Bist, H. D.; Brand, J. C. D.; Williams, D. R. *J. Mol. Spectrosc.* **1966**, *21*, 76.
(25) Lipert, R. J.; Colson, S. D. *J. Chem. Phys.* **1990**, *92*, 3240.
(26) Anderson, S. L.; Goodman, L.; Krogh-Jespersen, K.; Ozkabak, A. G.; Zare, R. N.; Zheng, C. *J. Chem. Phys.* **1985**, *82*, 5329.
(27) Kim, B.; Thantu, N.; Weber, P. M. *J. Chem. Phys.* **1992**, *97*, 5384.
(28) Schick, C. P.; Weber, P. M. *J. Phys. Chem. A* **2001**, *105*, 3735.
(29) Weber, P. M.; Stanks, J.; Thantu, N.; Hellmer, R. *J. Vac. Sci. Technol., A* **1992**, *10*, 408.
(30) Reid, K. L.; Field, T. A.; Towrie, M.; Matousek, P. *J. Chem. Phys.* **1999**, *111*, 1438.
(31) Kimura, K.; Katsumata, S.; Achiba, Y.; Yamazaki, T.; Iwata, S. *Handbook of HeI Photoelectron Spectra of Fundamental Organic Molecules*; Japan Scientific Societies Press: Tokyo, 1981.
(32) Kesper, K.; Diehl, F.; Simon, J. G. G.; Specht, H.; Schweig, A. *Chem. Phys.* **1991**, *153*, 511.
(33) Carpenter, S. D.; Schick, C. P.; Weber, P. M. *Rev. Sci. Instrum.* **1999**, *70*, 2262.
(34) Wu, M.; Taylor, D. P.; Johnson, P. M. *J. Chem. Phys.* **1991**, *94*, 7596.
(35) Agostini, P.; Fabre, F.; Mainfray, G.; Petite, G.; Rahman, N. K. *Phys. Rev. Lett.* **1979**, *42*, 1127.
(36) Kruit, P.; Kimman, J.; Muller, H. G.; van der Wiel, M. J. *Phys. Rev. A* **1983**, *28*, 248.
(37) Compton, R. N.; Miller, J. C. In *Laser Applications in Physical Chemistry*; Evans, D. K., Ed.; Marcel Dekker: New York, 1989; pp 221−306 and references therein.
(38) Kim, B.; Schick, C. P.; Weber, P. M. *J. Chem. Phys.* **1995**, *103*, 6903.
(39) Thantu, N.; Weber, P. M. *Z. Phys. D* **1993**, *28*, 191.
(40) Thantu, N.; Weber, P. M. *Chem. Phys. Lett.* **1993**, *214*, 276.
(41) Freed, K. F.; Nitzan, A. *J. Chem. Phys.* **1980**, *73*, 4765.
(42) Ondrey, G. S.; Rose, C.; Proch, D.; Kompa, K. L. *J. Chem. Phys.* **1991**, *95*, 7823.
(43) Rabalais, J. W. *Principles of Ultraviolet Photoelectron Spectroscopy*; John Wiley and Sons: New York, 1977.
(44) van Velzen, P. N. T.; van der Hart, W. J.; van der Greef, J.; Nibbering, N. M. M.; Gross, M. L. *J. Am. Chem. Soc.* **1982**, *104*, 1208.
(45) Walther, H. J.; Eyer, H.; Schlunegger, U. P.; Porter, C. J.; Larka, E. A.; Beynon, J. H. *Org. Mass Spectrom.* **1982**, *17*, 81.
(46) Russell, D. H.; Gross, M. L.; Nibbering, N. M. M. *J. Am. Chem. Soc.* **1978**, *100*, 6133.
(47) Trost, B.; Stutz, J.; Platt, U. *Atmos. Environ.* **1997**, *31*, 3999.
(48) Etzkorn, T.; Klotz, B.; Sorensen, S.; Patroescu, I. V.; Barnes, I.; Becker, K. H.; Platt, U. *Atmos. Environ.* **1999**, *33*, 525.
(49) Hammond, V. J.; Price, W. C.; Teegan, J. P.; Walsh, A. D. *Discuss. Faraday Soc.* **1950**, *9*, 53.
(50) Lipert, R. J.; Bermudez, G.; Colson, S. D. *J. Phys. Chem.* **1988**, *92*, 3801.